Journal of Materials Chemistry A

Tin-Based Ionic Chaperone Phases to Improve Low Temperature Molten Sodium-NaSICON Interfaces

Journal:	*Journal of Materials Chemistry A*
Manuscript ID	TA-ART-03-2020-003571.R1
Article Type:	Paper
Date Submitted by the Author:	26-May-2020
Complete List of Authors:	Gross, Martha; Sandia National Laboratories Small, Leo; Sandia National Laboratories Peretti, Amanda; Sandia National Laboratories Percival, Stephen; Sandia National Laboratories Rodriguez, Mark; Sandia National Laboratories, Spoerke, Erik; Sandia National Laboratories,

Tin-Based Ionic Chaperone Phases to Improve Low Temperature Molten Sodium-NaSICON Interfaces

Received 00th January 20xx,
Accepted 00th January 20xx

DOI: 10.1039/x0xx00000x

Martha M. Gross,[a] Leo J. Small,[a] Amanda S. Peretti,[a] Stephen J. Percival,[a] Mark A. Rodriguez[a] and Erik D. Spoerke*[a]

High temperature operation of molten sodium batteries impacts cost, reliability, and lifetime, and has limited the widespread adoption of these grid-scale energy storage technologies. Poor charge transfer and high interfacial resistance between molten sodium and solid-state electrolytes, however, prevents the operation of molten sodium batteries at low temperatures. Here, *in-situ* formation of tin-based chaperone phases on solid state NaSICON ion conductor surfaces is shown in this work to greatly improve charge transfer and lower interfacial resistance in sodium symmetric cells operated at 110 °C at current densities up to an aggressive 50 mA cm^{-2}. It is shown that static wetting testing, as measured by the contact angle of molten sodium on NaSICON, does not accurately predict battery performance due to the dynamic formation of a chaperone NaSn phase during cycling. This work demonstrates the promise of sodium intermetallic-forming coatings for the advancement of low temperature molten sodium batteries by improved mating of sodium-NaSICON surfaces and reduced interfacial resistance.

Introduction

There is an alarming shortage of safe, cost-effective, reliable grid-scale energy storage solutions needed to meet rapidly increasing worldwide demand.[1, 2] Molten sodium (Na) batteries offer great promise as one such energy storage system due to their high theoretical energy capacity and use of inexpensive and widely abundant materials.[3, 4] Widespread adoption of molten sodium batteries, however, has been dramatically limited by the high operating temperatures (~ 300 – 350 °C) necessary, in part, to achieve facile charge transfer between the molten sodium anode and the solid electrolyte separator needed for desirable battery performance.[3, 5] The development of tin (Sn)-based ionic "chaperone" phase coatings on NaSICON (Na Super Ion CONductor, $Na_3Zr_2Si_2PO_{12}$) ceramic separators presented in this work enables the cycling of molten sodium batteries at low temperatures by facilitating improved charge transfer across the interface between the molten sodium and the solid electrolyte. The enabling of low temperature operation of molten sodium batteries can unlock the promise of these systems, as lowering the operating temperature increases battery longevity, reduces materials cost, and increases safety, making these systems substantially more attractive for widespread adoption.[4, 6]

Traditional high temperature molten sodium batteries, such as Na-S or Na-$NiCl_2$, rely on the use of β"–Al_2O_3 solid electrolyte as a separator.[3, 5] Sodium beta batteries, as they are often called, suffer dramatically from the poor wetting of molten sodium on β"–Al_2O_3, a problem that is greatly exacerbated as the temperature drops below 250 °C.[5, 7-10] Wetting of molten sodium, as determined by the measurement of contact angle, is often discussed interchangeably with charge transfer.[7] As Fig. 1a shows, contact angle is often a reflection of the degree of physical contact between the molten sodium and the ceramic separator at their interface. A low contact angle of < 90° implies intimate contact between the Na and the ceramic surface, while a high contact angle (> 90°) implies poor contact at the Na-ceramic interface. As Fig. 1b shows, poor interfacial contact between the Na and the ceramic limits the surface area through with Na^+ ions can travel, which dramatically increases the interfacial resistance as cations such as Na^+ can only travel through localized "choke points" through the ceramic.[11-14]

One method to improve wetting on β"–Al_2O_3 has been the extensive application of coatings, such as Ni nanowires, porous carbons, porous iron oxide, Pb particles, Bi islands, and a screen-printed Pt grid.[9, 15-19] A second method that has been tested on β"–Al_2O_3, is alloying the Na anode with low melting temperature alkali metals or with other relatively low melting temperature metals, such as Bi or Sn, to improve wetting.[7, 9, 10, 15, 16, 19-21] Fig. S1[†] shows a comprehensive summary of previous work measuring Na wetting by contact angle to improve interfacial resistance. It can be seen in Fig. 1c, however, that there has been limited work undertaken to determine Na wetting below 150 °C. Results from literature demonstrate that the wetting of Na, as determined by the contact angle of Na on the ceramic, proves to be very poor at temperatures below 150 °C. The exception appears to be alloying Na with other low-melting temperature alkali metals (K, Rb, Cs).[9] Safety and stability are a concern with these alloys, however. K and Rb are capable of ion exchange with the Na^+ in β"–Al_2O_3, and the resulting volume expansion can cause the ceramic to fracture. Concerns about the safety of using the large mass of Cs necessary for grid-scale storage are noteworthy, in addition to its expense, due to its violent reactivity with water and formation of an explosive superoxide. For the time being, alloying Na with alkali metals to improve the wetting at low temperatures appears to be impractical for large scale applications.

Prior work on molten Na wetting has focused on the use of β"–Al_2O_3. In the case of low temperature (T < 150 °C) molten

[a] *Sandia National Laboratories, Albuquerque, NM 87185, USA.*
* Email: edspoer@sandia.gov
[†]Electronic Supplementary Information (ESI) available: See DOI: 10.1039/x0xx00000x

sodium batteries, however, NaSICON displays higher ionic conductivities compared to β"–Al_2O_3 at low temperature.[4, 10, 22]

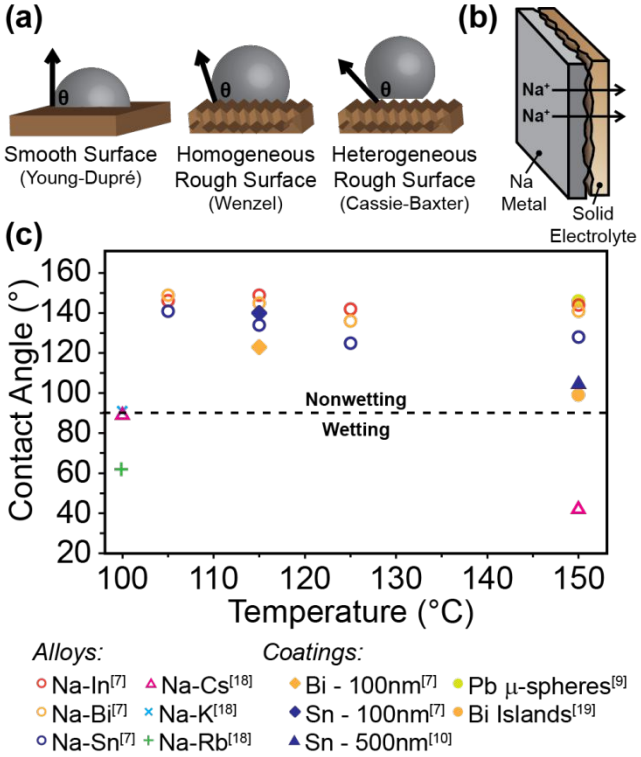

Fig. 1 Schematics of a) different contact angle models and b) incomplete wetting of Na on a solid electrolyte. c) Prior work of different methods to improve molten Na wetting by contact angle measurement in the temperature range of 100 – 150 °C. All work in this temperature range was performed on β"-Al_2O_3.

To date there have been few studies on the improvement of the interface between molten sodium and NaSICON at low temperature. One study used a deposited layer of indium tin oxide and another deposited graphene like carbon.[23, 24] In β"–Al_2O_3, the poor wetting of Na is often attributed to the high surface tension of molten Na, combined with the formation of Na_2O when molten Na reacts with adsorbed water on the surface of β"–Al_2O_3 or by the presence of surface Ca impurities leftover from synthesis.[9, 10, 19, 25, 26] It is unclear, however, if these mechanisms for poor wetting are applicable to NaSICON, which is synthesized in a very different manner and demonstrates substantially lower water reactivity than β"–Al_2O_3. The use of coatings made of alloying metals has shown promise as candidates for improving Na metal wetting on β"–Al_2O_3. It is, however, necessary to determine if such lessons can be applied to NaSICON. For this work Sn was chosen due to its favorably low solubility in Na at low temperatures, and due to work that previously looked at the use of Sn as an anode in room temperature Na^+-ion batteries.[7, 27, 28]

Here, Sn coatings of various thicknesses on NaSICON are investigated for the purposes of enhancing interfacial contact and charge transfer between molten sodium and the solid electrolyte at 110 °C. We demonstrate the dramatic lowering of overpotential in molten sodium symmetric cells with a NaSICON separator by the application of these Sn coatings. Furthermore, we show that wettability as measured by contact angle is an incomplete predictor of battery performance due to the dynamic formation of a Na^+ ion-conducting NaSn chaperone phase. This work opens up a new area of research towards the exploration of sodium intermetallic-forming metal coatings on NaSICON for improved molten sodium battery performance at low temperatures.

Experimental Section

NaSICON Preparation

NaSICON ($Na_3Zr_2Si_2PO_{12}$) precursor powder was synthesized by combining zirconium (IV) silicate ($ZrSiO_4$, Sigma Aldrich, -325 mesh) and sodium phosphate tribasic dodecahydrate ($Na_3PO_4 \cdot 12\ H_2O$, Sigma Aldrich, ≥ 98 %) in, respectively, a 2 : 1 molar ratio. The mixture was ball-milled for 12 h with ~ 1/3 of the final volume of zirconia milling media and 1/3 of the final volume of ethanol. The resulting mixture was cleaned from the milling media with ethanol, dried with a rotary evaporator to remove the bulk ethanol, and further dried under vacuum overnight.
The NaSICON precursor powder was calcined at 600 °C for 2 hours in air. Once cooled to 100 °C the calcined powder was immediately moved to a dry nitrogen purge box, ground with a mortar and pestle, sifted, and poured into 1.125 inch die for pressing to 10 kpsi. The pressed cylinder was buried in NaSICON precursor powder containing a 5 % excess of Na_3PO_4, within a β-Al_2O_3 crucible and covered before sintering in air at 1230 °C for 12 h with a 5 °C min^{-1} ramp and cooling rate. After sintering, the cylinder was sliced into approximately 1 mm thick disks using a low speed diamond blade saw. NaSICON disks used for sessile drop testing were polished on one surface to P2500 grit. NaSICON disks used for symmetric cell testing were polished to 0.8 – 0.9 mm thickness at P2500 grit on both sides.

Sn Coating Preparation

Sn coatings were achieved by radio frequency (RF) magnetron sputtering using a Kurt J. Lesker Lab 18 thin film deposition system and a pure Sn target (99.99%, SCI Engineering Materials, 3 inch diameter). Deposition was performed under 5 mTorr argon, an output power of 200 W, and no intentional substrate heating. Polished NaSICON disks for wetting tests were coated with Sn on one side, while NaSICON disks for symmetric cells were coated on both sides to the specified thickness. Glass slides were coated with Sn on one side for profilometry and cross-sectional SEM for determination of Sn thickness.

Wettability Test

Wettability testing was performed by the sessile drop technique. All wettability tests were performed in a glovebox under an Ar atmosphere. Both a piece of NaSICON and Na metal were heated on an Al block to 110°C. Molten Na was transferred to the NaSICON surface using a heated glass pipette. Contact angles were measured after 30 minutes.

Materials Characterization

Analysis of the surface morphology, composition by energy-dispersive x-ray spectroscopy (EDX), and thickness of Sn coatings was performed with a Zeiss Supra 55VP scanning electron microscope (SEM) at 10 kV. Surface morphology was

analyzed on Sn-coated NaSICON. Sn coating thickness was determined analysis of coatings on glass slides which were scored and cleaved to expose the Sn coating cross-section. Phase identification of as-deposited Sn coatings on NaSICON was performed by x-ray diffraction (XRD), using a Bruker D2 Phaser diffractometer with Cu Kα radiation. XRD of samples exposed to molten sodium, including wetting tests and cycling in symmetric cells, was performed using a Siemens D500 diffractometer with Cu Kα radiation and custom beryllium dome chamber, described previously, to prevent exposure to ambient atmosphere.[29] Samples were mounted on an Al stub using pure Na in an argon-filled glovebox and sealed in the Be dome chamber before XRD analysis was performed. Profilometry was performed on Sn-coated glass slides using a Dektak 6M profilometer.

Symmetric Cell Assembly and Testing

Cells were assembled in a planar configuration using custom glass cell parts. A schematic and a picture of the assembly can be found in Fig. S2.† Glass chambers were sealed with a tungsten rod current collector and filled with 4 g of molten sodium (Alfa Aesar, 99.8%, further purified by melting to remove surface oxidation) and cooled. A piece of NaSICON, with or without Sn coating, was placed between two filled chambers and the cell was sealed with EPDM O-rings (McMaster-Carr). Geometric area of the NaSICON was 1.76 cm^2. Cells were assembled in a glovebox under an argon atmosphere. After assembly, the cell was placed in a 110°C oven for testing.
Electrochemical impedance spectroscopy (EIS) of symmetric cells was carried out using a Solartron ModuLab MTS analyzer at a frequency range of 1 MHz to 10 mHz, and at 0 V DC with respect to the open circuit potential. Symmetric cells were analyzed under an AC amplitude of 10 mV. Cycling tests were performed using an Arbin battery cycler, during which cells were charged and discharged for 1 h each at the specified current density. Each cell was cycled for 5 cycles at a given current density, starting at 0.5 mA cm^{-2} and increasing to 1, 2, 5, 10, 25, and 50 mA cm^{-2}. Current density and resistance were determined based on geometric area of the NaSICON.

Results and Discussion

In order to better understand the phase evolution of the Na-Sn-NaSICON interphase and its influence on interfacial resistance and practical battery performance, a series of NaSICON samples were prepared with Sn coatings systematically varied in thickness from 0 to 700 nm, and characterized by scanning electron microscopy (SEM), contact angle, x-ray diffraction (XRD), electrochemical impedance spectroscopy (EIS), and symmetric cell cycling.

Sn coatings were deposited by radio frequency (RF) magnetron sputtering and pure Sn phase was confirmed by XRD and EDX (Fig. S3-5)†. Coating thickness was measured by profilometry and SEM of the cross-section of Sn coatings on glass slides. Actual measured values of coating thickness based on profilometry and direct measurement from SEM (Fig. 2) show some variation due to surface roughness, but it can be estimated that the thicknesses of the dense portion of the coating (neglecting rough surface features) are nominally 40 nm, 170 nm, 500 nm, and 700 nm. Notably, the 700 nm film showed significant variability to as thick as 1030 nm. Critically, however, all values are considered to be substantially above or below the critical thickness of Sn as determined by the solubility limit of Sn in molten Na at 110 °C, discussed later. Fig. 2 shows representative images of the Sn coatings at each thickness. Each of the Sn coatings, as deposited, exhibit substantial roughness in their surface morphology, with surface roughness increasing with increasing coating thickness. SEM of the coating cross-section shows that the 40 nm coatings are non-conformal, with some bare patches of substrate on the order of a few nanometers. All other coatings cover the substrate surface completely. Representative EDX maps confirming the Sn coating on a NaSICON substrate are shown in Fig. S4 and S5. †

As previously discussed, there have been limited studies to date on the wetting of molten sodium on NaSICON solid electrolytes, and no studies have been performed previously at low temperatures (< 150 °C). Previous work to improve molten

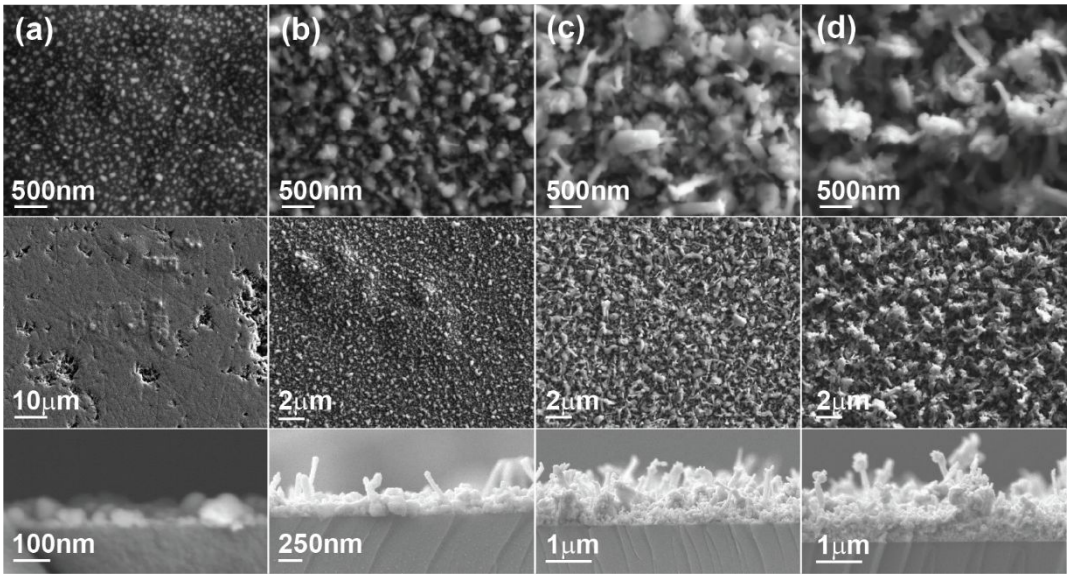

Fig. 2 SEM images of a) 40 nm, b) 170 nm, c) 500 nm, and d) 700 nm thick Sn coating on NaSICON.

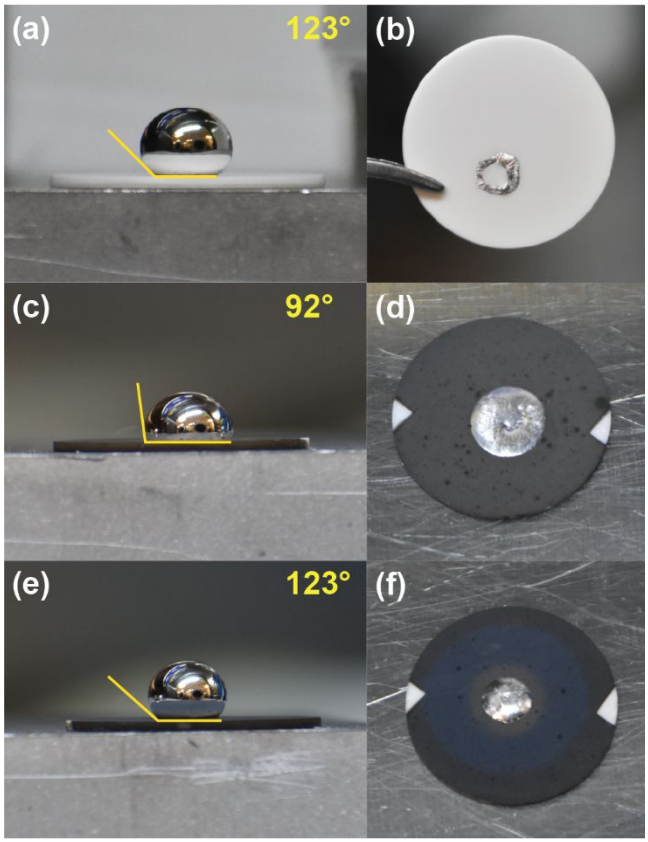

Fig. 3 a, c, e) Contact angle measurements and b, d, f) images of NaSICON after measurement. a, b) Bare NaSICON. c, d) NaSICON with Sn coating below critical thickness. e, f) NaSICON with Sn coating above critical thickness.

Na wetting on β"–Al_2O_3 has discussed the importance of the "critical thickness" of a coating, in relation to coatings made of metals that are partially soluble in molten sodium.[10, 19] Critical thickness is the thickness above which the metal coating exceeds it solubility limit in the molten sodium, at which point a layer of the metal coating remains after contact with the molten sodium. Previous work has either used metal coatings below the critical thickness or developed island- or grid-type coating structures so as to prevent depositing a metal blocking layer on the ceramic surface.[7, 9, 10, 18, 19] In this work, a layer of Sn was deposited at thicknesses both above and below the critical thickness, as determined by the solubility of Sn. The solubility limit of Sn at 110°C was calculated to be 6.7 x 10^{-3} wt% Sn using the FactSage 7.4 FTlite database.[24, 30] For contact angle measurements taken by sessile drop technique, the critical thickness was estimated to be 100 nm. For symmetric cells, discussed later, the critical thickness was estimated to be 220 nm, due to the larger mass of sodium and increased contact area.

Wettability of the molten Na on the NaSICON was determined by the sessile drop technique, in which the contact angle of the molten Na drop was measured on bare NaSICON and on Sn-coated NaSICON, in which the Sn coating thickness was below and above the critical thickness. A contact angle of < 90° is considered to demonstrate wetting of the liquid to the solid surface, while a contact angle of > 90° is considered to be nonwetting. Fig. 3a shows that at 110°C, molten sodium wet poorly to bare NaSICON and achieved a best contact angle of 123°. Below the critical thickness, molten Na achieved a best contact angle of 92°, while above the critical thickness, molten Na achieved a contact angle similar to that on bare NaSICON as shown in, respectively, Fig. 3c and 3e. This angle is also similar to that achieved with a molten Na-Sn alloy on bare NaSICON, shown in Fig. S6.† Interestingly, Sn coatings exhibited a slight color change after deposition of the Na drop, seen most clearly in Fig. 3f as a ring of blue around the Na. Literature indicates a possible sodiation of the Sn,[31] but XRD was unable to reveal any new phase formation, as is further illustrated in Fig. 6. Removal of the Na drop further demonstrates the poor wetting of the Na on bare NaSICON, shown in Fig. 3b, as most of the Na was easily removed. Na was difficult to remove from both Sn-coated

NaSICON coupons, regardless of Sn thickness, as shown in Fig. 3d and 3f. In sum, Sn coatings below the critical thickness enhanced Na wetting on NaSICON, while those above the critical thickness did not change the contact angle as compared to bare NaSICON.

Wettability testing was performed, as contact angle is typically used as a method of screening different materials and approaches to improve wetting of molten sodium to a solid electrolyte. It is typically reasoned that improvement in the contact angle should correlate to decreased interfacial resistance and overall battery performance. The primary goal of this and other work, however, is not explicitly improved contact angle but instead improved charge transfer and lower interfacial resistance in a molten sodium battery. With this in mind, symmetric cells were assembled using bare NaSICON and Sn-coated NaSICON to verify that the improved wettability observed in the contact angle testing correlated to lowered interfacial resistance and improved battery performance. Symmetric cells were tested with Sn coatings at thicknesses above (500 nm, 700 nm) and below (40 nm, 170 nm) the estimated critical thickness of 220 nm at 110°C.

Symmetric cells were cycled at different current densities to determine the effect of Sn-coated NaSICON on battery performance. Cells were cycled for 5 cycles at each current density, starting at 0.5 mA cm^{-2} and increasing up to 50 mA cm^{-2}. As can be seen in Fig. 4, the application of a Sn coating on NaSICON substantially lowers the overpotential of a symmetric cell compared to one assembled with bare NaSICON. Moreover, the presence of Sn stabilizes the cycling behavior. Whereas bare NaSICON displayed a charging voltage higher on the first cycle than subsequent cycles, Sn-coated NaSICON displayed a consistent charge-discharge profile. Analysis of the NaSICON after cycling, seen in Fig. S7,† shows that Sn-coated NaSICON demonstrates excellent wetting to the Na compared to bare NaSICON, regardless of Sn coating thickness. Contrary to what was expected from the static contact angle testing, overpotential decreases with increasing Sn coating thickness; cells with coatings above the critical thickness (500 nm, 700 nm) show better performance compared to cells with coatings

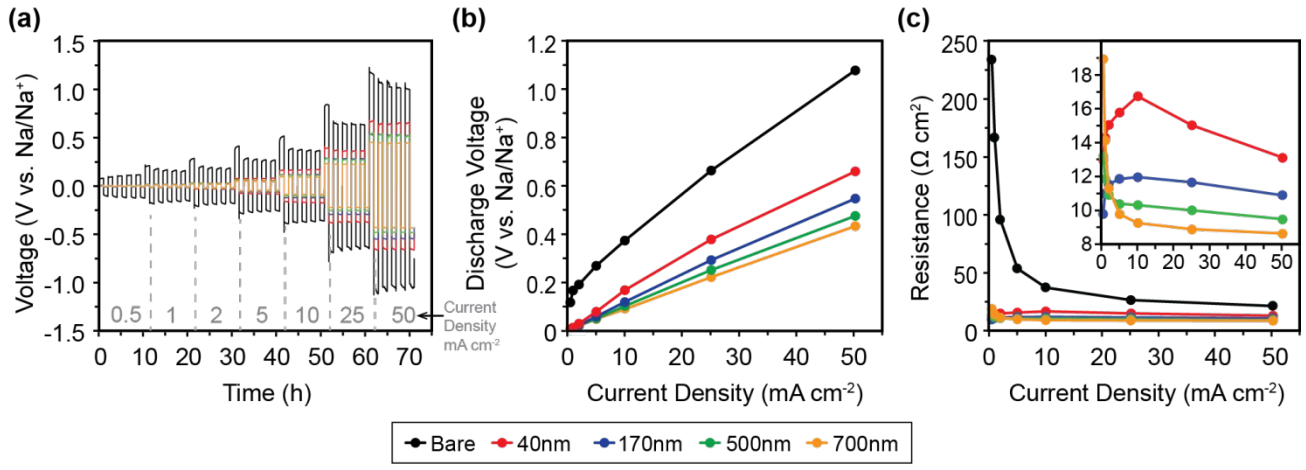

Fig. 4 a) Voltage cycling profile, b) Average discharge voltage at different current densities, and c) Resistances obtained by DC measurement of symmetric cells assembled with bare and Sn-coated NaSICON.

below the critical thickness (40 nm, 170 nm). From the contact angle testing alone, it would have been expected that very thick layers of Sn would have demonstrated large overpotentials due to poor wetting of the Na. Furthermore, a thick layer of Sn present at the interface would have been expected to act as a blocking layer, preventing the transport of Na^+ ions as has been demonstrated previously with conformal Bi coatings.[19] Instead, our results show that cells with thick Sn coatings above the critical thickness perform better than those with Sn coatings below the critical thickness.

As one measure of charge transfer, impedance spectroscopy was performed on all symmetric cells before and after cycling. Characteristic Nyquist plots are shown in Fig. 5. Generally, impedance spectra were offset along the Z' axis and display one

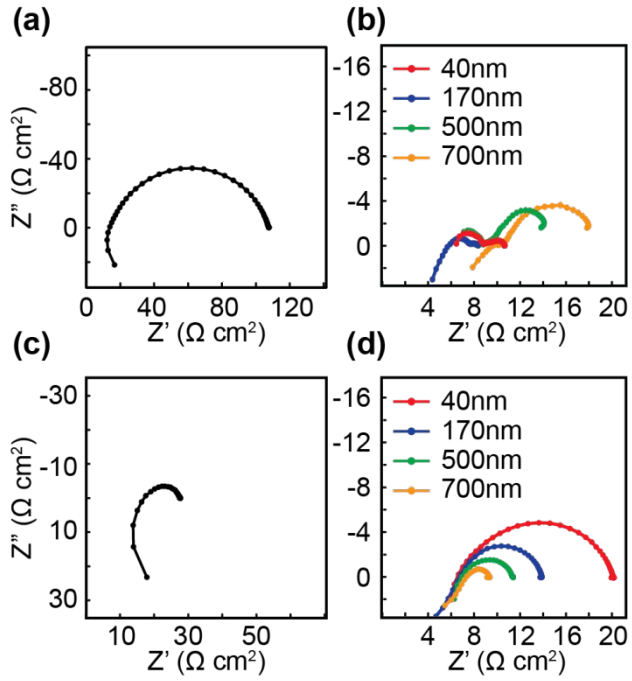

Fig. 5 Impedance of symmetric cells a, b) before and c, d) after cycling assembled with with a, c) bare NaSICON and b, d) Sn-coated NaSICON.

or two semicircles in the complex impedance plane. This offset, related to the series resistance of the cell, is dominated by the NaSICON separator, but also includes the tungsten current collector, Na metal, and any bulk Sn-like coating on the NaSICON. The widths of the semicircles are attributed to charge transfer resistances across the Na-NaSICON interface. The process used to determine these measures is illustrated in Fig. S8.† Thus, small semicircles with a small offset (i.e. closer to 0,0) are indicative of low resistances and superior cell performance. Before cycling, shown in Fig. 5a and 5b, a marked difference is seen between cells with or without a Sn coating. For cells assembled with bare NaSICON (no Sn coating), one large semicircle 53 Ω in diameter is seen, displaced 7.9 Ω along the Z' axis. The large semicircle diameter is attributed to a large interfacial charge transfer resistance between the Na and the NaSICON. The Z' axis offset is over double the resistance expected for NaSICON, implying poor surface contact between the molten Na and the NaSICON, as would be expected based on the contact angle measurements.

The addition of a Sn coating to the NaSICON separator in an uncycled cell not only decreases the semicircle diameter by an order of magnitude, but also lowers the Z'-axis offset by more than a factor of two. That is to say, the Sn coating decreases both the interfacial charge transfer resistance as well as the series resistance of the cell. This series resistance of ~ 3.4 Ω is on par with that expected for NaSICON bulk and grain boundary resistances, implying improved surface contact with the NaSICON. While this performance is expected for Sn coatings below the critical thickness from contact angle testing, we see a similar trend for Sn coatings above the critical thickness as well. This trend implies that despite poor contact angles, molten sodium still achieves a good surface contact on the Sn-coated NaSICON. It is important to note that upon adding a Sn coating, another semicircle appears in the Nyquist plot. This additional semicircle is attributed to the replacement of the Na-NaSICON interface with the Na-Sn and Sn-NaSICON interfaces. Overall, these two interfacial resistances sum to much less than that of the Na-NaSICON interfacial resistance seen in the case of bare NaSICON (~ 3 versus ~ 53 Ω). Thus, the Sn coating decreases the resistance of the system by both improving contact area by over a factor of two and decreasing the charge transfer resistance of the Na-NaSICON interface by greater than a factor of ten. Further details about the measured resistances before and after cycling can be found in Fig. S9 and Table S1.†

After cycling, shown in Fig. 5 and 5d, cells assembled with bare NaSICON demonstrate a larger series resistance, shown by a shift in the impedance spectra to a more positive position along the Z' axis. This indicates no improvement to the contact area between the Na and the NaSICON during battery cycling. A decrease in the semicircle diameter occurred, indicating improved charge transfer. Cells assembled with Sn-coated NaSICON, regardless of Sn coating thickness, see the two semicircles present before cycling change to a single semicircle after cycling. This change suggests an evolution of the structure at the Na-NaSICON interface. As the Sn thickness increases from 40 nm to 700 nm, a clear trend is observed: the width of the semicircle decreases, while simultaneously shifting more positive along the Z' axis. This is interpreted to mean that the charge transfer resistance across the Na-NaSICON interface decreases, while the series resistance of the cell modestly increases. Thus, increasing the starting Sn thickness effectively decreased the interfacial resistance of the Na-NaSICON interface after cycling. At the same time, increasing the Sn thickness modestly increased the series resistance of the cell by adding another highly conductive phase that the ions must pass through during cycling. This can be envisioned as a low resistance ionic chaperone phase, which facilitates the Na^+ ion transfer between the NaSICON and the Na metal.

Air-sensitive XRD measurements were taken of the cycled Sn-coated NaSICON to characterize the NaSn chaperone phase. As Fig. 6 shows, XRD reveals the formation of the intermetallic phase NaSn. Identifying NaSn peaks are indicated by the orange diamonds. Based on this evidence, we conclude that the excess Sn forms a sodium ion-conducting intermetallic phase, rather than a blocking layer, on the surface of the NaSICON. No clear evidence of intermetallic formation was detected by XRD for static wetting tests, which may be due to the slow kinetics of sodiation when no bias is applied.[31] This further indicates a dynamic formation of NaSn during symmetric cell cycling, rather than a spontaneous sodiation of the Sn simply by contact with the molten Na. Interestingly, though both the 500nm and 700nm coating are above the critical thickness, we continue to see an improvement in the 700nm coating over the 500nm coating. As can be observed in Fig. S7, while the 500nm and 700nm coatings both exhibited excellent wetting, there are still some regions where the NaSICON was not *fully* wet in the 500nm coating symmetric cells. We surmise that incomplete wetting is related to the observed lower performance, possibly due to reduced Sn solubility on less optimally-wetted surfaces.

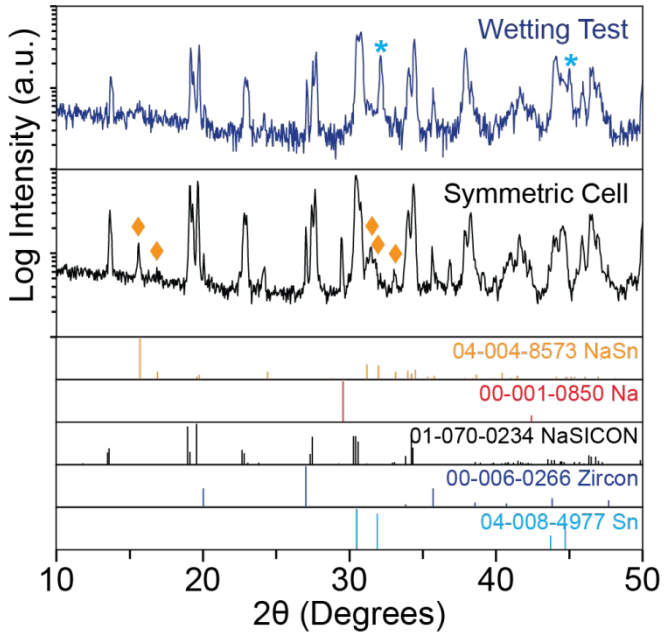

Fig. 6 XRD of NaSICON with 700nm Sn coating after static wetting testing and after dynamic cycling in a symmetric cell compared to powder diffraction files (PDF). Blue stars highlight identifying Sn peaks and orange diamonds highlight identifying NaSn peaks.

Conclusions

This work demonstrates for the first time the successful use of Sn coatings to lower the charge transfer resistance of molten sodium on NaSICON at the low temperature of 110°C. It is further demonstrated that in the case of the Sn system, poor wetting of Na on thick Sn coatings (above the critical thickness in which the solubility limit of Sn in molten Na is reached with a Sn layer remaining) does not correlate to battery performance, and in fact thick Sn coatings performed better than thin Sn coatings. It was determined that Sn did not form an ionic blocking layer owing to the dynamic formation of the NaSn intermetallic. This intermetallic acts as a Na^+ ion-conducting layer on the surface of the NaSICON, decreasing interfacial resistance by more than an order of magnitude, and drastically decreasing the voltage required to drive a symmetric Na-NaSICON-Na cell at 50 mA cm^{-2}. This work shows the promise of exploring intermetallic-forming coatings as a path towards lowering the interfacial resistance between molten Na and NaSICON at 110 °C. Correlating improvements in low temperature battery performance are the key in improving the widespread utility of this important emerging energy storage technology.

Conflicts of interest

There are no conflicts to declare.

Acknowledgements

The authors would like to thank Luis Jauregui and Sara Dickens for recording SEM micrographs of Sn coatings. This work was supported by the U.S. Department of Energy Office of Electricity Energy Storage Program, managed by Dr. Imre Gyuk. Sandia National Laboratories is a multimission laboratory managed and operated by National Technology & Engineering Solutions of Sandia, LLC, a wholly owned subsidiary of Honeywell International Inc., for the U.S. Department of Energy's National Nuclear Security Administration under contract DE-NA0003525. This paper describes objective technical results and analysis. Any subjective views or opinions that might be expressed in the paper do not necessarily represent the views of the U.S. Department of Energy or the United States Government.

References

1. S. Sorrell, *Renewable Sustainable Energy Rev.*, 2015, **47**, 74-82.
2. H. Safaei and D. W. Keith, *Energy Environ. Sci.*, 2015, **8**, 3409-3417.
3. K. B. Hueso, M. Armand and T. Rojo, *Energy Environ. Sci.*, 2013, **6**, 734-749.
4. L. J. Small, A. Eccleston, J. Lamb, A. C. Read, M. Robins, T. Meaders, D. Ingersoll, P. G. Clem, S. Bhavaraju and E. D. Spoerke, *J. Power Sources*, 2017, **360**, 569-574.
5. K. B. Hueso, V. Palomares, M. Armand and T. J. N. R. Rojo, *Nano Res.*, 2017, **10**, 4082-4114.
6. H.-J. Chang, X. Lu, J. F. Bonnett, N. L. Canfield, S. Son, Y.-C. Park, K. Jung, V. L. Sprenkle and G. Li, *Adv. Mater. Interfaces*, 2018, **5**, 1701592.
7. K. Ahlbrecht, C. Bucharsky, M. Holzapfel, J. Tübke and M. J. Hoffmann, *Ionics*, 2017, **23**, 1319-1327.
8. M. Holzapfel, D. Wilde, C. Hupbauer, K. Ahlbrecht and T. Berger, *Electrochim. Acta*, 2017, **237**, 12-21.
9. X. Lu, G. Li, J. Y. Kim, D. Mei, J. P. Lemmon, V. L. Sprenkle and J. Liu, *Nat. Commun.*, 2014, **5**, 4578.
10. D. Reed, G. Coffey, E. Mast, N. Canfield, J. Mansurov, X. Lu and V. Sprenkle, *J. Power Sources*, 2013, **227**, 94-100.
11. W. Zhou, Y. Li, S. Xin and J. B. Goodenough, *ACS Cent. Sci.* , 2017, **3**, 52-57.
12. K. Fu, Y. Gong, B. Liu, Y. Zhu, S. Xu, Y. Yao, W. Luo, C. Wang, S. D. Lacey, J. Dai, Y. Chen, Y. Mo, E. Wachsman and L. Hu, *Sci. Adv.*, 2017, **3**, e1601659.
13. M. J. Wang, R. Choudhury and J. Sakamoto, *Joule*, 2019, **3**, 2165-2178.
14. S. Wei, S. Choudhury, Z. Tu, K. Zhang and L. A. Archer, *Acc. Chem. Res.*, 2018, **51**, 80-88.
15. Y. Hu, Z. Wen, X. Wu and Y. Lu, *J. Power Sources*, 2013, **240**, 786-795.
16. Y. Hu, Z. Wen, X. Wu and J. Jin, *J. Power Sources*, 2012, **219**, 1-8.
17. Y. Hu, Z. Wen and X. Wu, *Solid State Ionics*, 2014, **262**, 133-137.
18. H.-J. Chang, X. Lu, J. F. Bonnett, N. L. Canfield, K. Han, M. H. Engelhard, K. Jung, V. L. Sprenkle and G. Li, *J. Mater. Chem. A*, 2018, **6**, 19703-19711.
19. D. Jin, S. Choi, W. Jang, A. Soon, J. Kim, H. Moon, W. Lee, Y.

Lee, S. Son, Y.-C. Park, H. Chang, G. Li, K. Jung and W. Shim, *ACS Appl. Mater. Interfaces*, 2019, **11**, 2917-2924.

20. H. Liu, X.-B. Cheng, J.-Q. Huang, S. Kaskel, S. Chou, H. S. Park and Q. Zhang, *ACS Mater. Lett.*, 2019, **1**, 217-229.
21. C. Wang, H. Xie, L. Zhang, Y. Gong, G. Pastel, J. Dai, B. Liu, E. D. Wachsman and L. Hu, *Adv. Energy Mater.*, 2018, **8**, 1701963.
22. S. Song, H. M. Duong, A. M. Korsunsky, N. Hu and L. Lu, *Sci. Rep.*, 2016, **6**, 32330.
23. L. Xue, T. G. Tucker and C. A. Angell, *Adv. Energy Mater.*, 2015, **5**, 1500271.
24. E. Matios, H. Wang, C. Wang, X. Hu, X. Lu, J. Luo and W. Li, *ACS Appl. Mater. Interfaces*, 2019, **11**, 5064-5072.
25. L. Viswanathan and A. V. Virkar, *J. Mater. Sci.*, 1982, **17**, 753-759.
26. M. W. Breiter, N. S. Choudhury and E. L. Hall, *Solid State Ionics*, 1984, **14**, 225-230.
27. Z. Tu, S. Choudhury, M. J. Zachman, S. Wei, K. Zhang, L. F. Kourkoutis and L. A. Archer, *Nat. Energy*, 2018, **3**, 310-316.
28. H. Kim, H. Kim, Z. Ding, M. H. Lee, K. Lim, G. Yoon and K. Kang, *Adv. Energy Mater.*, 2016, **6**, 1600943.
29. M. A. Rodriguez, T. J. Boyle, P. Yang and D. L. Harris, *Powder Diffr.*, 2008, **23**, 121-124.
30. FactSage 7.4 FTlite Database, http://www.crct.polymtl.ca/fact/documentation/, (accessed October 2019)
31. J. S. Gutiérrez-Kolar, L. Baggetto, X. Sang, D. Shin, V. Yurkiv, F. Mashayek, G. M. Veith, R. Shahbazian-Yassar and R. R. Unocic, *ACS Appl. Energy Mater.*, 2019, **2**, 3578-3586.

Table of Content Entry for:

Tin-Based Ionic Chaperone Phases to Improve Low Temperature Molten Sodium-NaSICON Interfaces

M.M. Gross, L.J. Small, A.S. Peretti, S.J. Percival, M.A. Rodriguez, E.D. Spoerke*

A novel NaSn intermetallic improves critical electrochemical interfaces between molten sodium and NaSICON ceramic electrolyte at low temperatures (110 °C).